Construction and Building Materials 440 (2024) 137402

Contents lists available at ScienceDirect

Construction and Building Materials

journal homepage: www.elsevier.com/locate/conbuildmat

Development of a robust and precise methodology for the measurement of the radon diffusion coefficient in diverse materials

E. Castaño-Casco *, I. Gutiérrez-Álvarez, A. Barba-Lobo, J.P. Bolívar

Radiation Physics and Environment Group (FRYMA), Centre for Natural Resources, Health and Environment (RENSMA), University of Huelva, Huelva 21007, Spain

ARTICLE INFO

Keywords:
Radon
Radon indoors
Radon diffusion coefficient
Building materials

ABSTRACT

The main sources of radon indoors are the infiltration from the soil through the building materials and the materials themselves. These pathways are significantly influenced by the radon diffusion coefficient, *D*, of those elements, playing an important role when trying to mitigate radon accumulation. Current methodologies developed to determine *D* are difficult to apply. ISO 11665-13 imposes restrictive conditions on the experimental system and requires the application of numerical methods. In the methodology the problem material is placed between a chamber containing a radon source and an empty one and radon concentration is measured in the chambers. The *D* closer to the experimental data is then selected. In this work, the methodology was improved, and an algorithm was developed to complement the ISO. The algorithm solves for the physical governing equations and finds the value of *D* that best fits the data by minimising the differences between the predicted and experimental concentrations. Various statistical parameters and stop conditions were studied to determine when an optimal *D* was found. A validation procedure was developed for internal validation, and results were compared with the literature for external validation. Additional results are presented for materials not found in the literature.

1. Introduction

One of the main contributors to the effective dose from natural radioactivity in the Earth crust is the ^{238}U-series radionuclides, which produces ^{222}Rn ($T_{1/2}$ = 3.8 d). Given that this radionuclide is a noble gas, it can easily escape into the atmosphere from the surface soils in which it is generated, then it decays to its short-life decay products that can adhere onto the respiratory system when they are inhaled. Radon gas and its short half-life decay products, ^{218}Po ($T_{1/2}$ = 3.1 min), ^{214}Pb ($T_{1/2}$ = 26.8 min), ^{214}Bi ($T_{1/2}$ = 19.9 min) and ^{214}Po ($T_{1/2}$ = 164.3 μs), are responsible of almost half of the effective dose received by the public from natural sources [1–3], and their long-term inhalation under high concentrations can cause lung cancer [4–7]. In the open air, radon gas is diluted and transported in the atmosphere [8–10] and is found at low concentrations, around 10 $Bq\ m^{-3}$, but in enclosed spaces such as mines [11,12] or buildings [13–16], it can accumulate and reach high levels (2–3 orders of magnitude higher), increasing the importance of studying indoor air quality [17–19].

The European Directive 2013/59/EURATOM [20] includes the obligation to reduce the public exposure to radon, requiring Member States to elaborate national plans against radon and to establish a national reference value for radon concentration in close buildings, with the reference value being an annual average of less than 300 $Bq\ m^{-3}$. It also states the need to identify residences, buildings with public access and workplaces, in which the annual average value for radon concentration is higher than the reference value, to consider any possible entry point for radon gas and to adopt measures to reduce the radon concentration [21,22].

The main source of indoor radon [23,24] is the infiltration from the soil of the building basement, through cracks and crevices, or by diffusion through the construction elements [25–28]. The building materials themselves, depending on their radioactive composition [29,30], can also generate radon and release it into the indoor air [31–35]. The radon diffusion coefficient of the different building materials will be the parameter that regulates the transport of radon through them and will have a greater effect on the flux through the internal surface of buildings. Consequently, this parameter has to be considered when studying the possible accumulation of radon indoors [36].

Several methods have been developed to determine the radon diffusion coefficient of materials [37,38].

* Corresponding author.
E-mail address: elena.castano@dci.uhu.es (E. Castaño-Casco).

https://doi.org/10.1016/j.conbuildmat.2024.137402
Received 10 April 2024; Received in revised form 28 May 2024; Accepted 7 July 2024
Available online 15 July 2024

Cozmuta and Van Der Graaf [39] and Ye et al. [40] considered the stationary state and obtained the radon diffusion coefficient by studying the radon exhalation rate from one side of the material, being the main drawback of this methodology its experimental setup, specifically the necessity to reshape the material [39,40] and the difficulty to find a cover against radon [39]. Other methods used indirect measurements [41–43]. Arafa [41] employed activated charcoal canisters, which were covered with the problem material and exposed to a known radon concentration, but it is important to ensure that the canister is properly prepared so that the radon absorption capacity is not affected. Quindos [42] and Tsapalov et al. [43] covered one side of a modified Lucas cell with the material of study. From the approach taken to solve the equations involved in the problem there is a limitation in the thickness of the material and range of the radon diffusion coefficient [42] or the necessity of an special software [43].

The ISO 11665-13 "Determination of the diffusion coefficient in waterproof materials: membrane two-side activity concentration test method" [44], which is based on the work of Jiránek & Svoboda [45], relies on measuring the radon concentration in two chambers separated by the problem material. A radon source is placed in one of the chambers and the other one is kept empty, measuring the radon concentration evolution in both chambers. They proposed two different approaches.

The first one is a steady state method that is easier to apply but longer to test, and it is necessary to estimate beforehand the time needed to reach the stationary state. Under steady-state conditions and neglecting radon radioactive decay, back diffusion and ventilation, the exhalation can be calculated as the slope of the linear regression of the concentration in the empty chamber versus time. An equation for the exhalation, dependent on the radon diffusion coefficient and obtained through solving the steady-state diffusion transport in the material, is then compared with the previously calculated value, and the radon diffusion coefficient is found by an iterative process. This approach is less accurate as many approximations are made.

The second one is a non-steady stage approach, where the diffusion equation is numerically solved and the radon concentration in the empty chamber is calculated for different values of the diffusion coefficient. Afterwards, the value of the diffusion coefficient with the radon concentration in the empty chamber that best fits the experimental data is selected as the result.

When replicated by other studies [46–48] the first method, the steady state case, is usually chosen even though it has more approximations, as the non-steady state solution is not trivial to be applied. The work of Szajerski & Zimny [49] is based on the same methodology, but they only make measurements in the empty chamber, which requires a prior characterization of the radon source. They solve the transient state by a numerical solution using the software SCILAB. Tejado-Ramos et al. [50] also applies the ISO two-chamber method in the non-stationary state applying a numerical solution with a GNU octave script. They use more affordable radon detectors which causes a limitation in the thickness of the material and the radon diffusion coefficient. The numerical methods applied in [49] and [50] for solving the problem are not made available since they are not the main subject of these studies.

The main issue with a simple and accurate application of the ISO [44] methodology is the resolution of the diffusion problem to find the best fitting radon diffusion coefficient, D. There is existing license software [51] that tests different values of D given by the user as an input and selects the one that give results closer to the measurements. But, to the best of our knowledge, there is no current open-source option available. The methodology also establishes long term measurements and restrictive conditions for the measurement system.

For those reason, in this work, the numerical solution applied to obtain D is done through a developed code, being this open-source search algorithm the main contribution in this work. The algorithm searches for the optimal value of D, using the experimental measurements as a reference, through various statistical parameters. This makes the iterative process faster and easier as we minimise one parameter to actively search for the best D value, and even if the algorithm starts with a non-optimal value, the program will select new values in the right direction in subsequent iterations. Some improvements have also been made to the methodology to make it easier and faster to apply.

Taking into account the previous defined problem, the main objective of this study was to develop and apply a new algorithm to obtain the radon diffusion coefficient of materials that is easy to replicate and apply by a general user. The developed algorithm, Radco, can be found on the website of the Nuclear Safety Council (CSN), as it is part of a project funded by them. Also, the experimental set-up that complements this algorithm is easily adaptable to different construction materials.

2. Theory and methods

2.1. Theoretical framework

The main idea of the proposed method by the ISO [44] is to place the problem material between two chambers, one of which will be empty ("receiver container"), and another one will contain a radon source ("source container") (Fig. 1). The different concentrations between the two chambers will cause a transport of radon through the material separating them. Measuring the time evolution of the radon concentration in the chambers allows to calculate the radon diffusion coefficient.

2.1.1. Radon transport through the problem material

Some assumptions have been made in the equation that regulates the transport of radon in the material under study. The transport of radon is only considered in one dimension, along the x-axis in the direction from the source container to the receiver container, as the material is homogeneous, making the transport linear. Diffusion is assumed to be the only mechanism for transport [52], so other transport mechanisms, such as the advection given by Darcy's law [53], are neglected. This is a reasonable approximation as we have laboratory conditions, with small changes in temperature, pressure, and humidity, which allows for the pressure driven transport to be ignored. In addition, the only sink term consider is the radon decay and the initial radon in the air of the containers is neglected [54]. Considering all these assumptions, the governing equation for the radon concentration in the material existing between the chambers is [53,55]:

$$\frac{\partial C(x,t)}{\partial t} = D\frac{\partial^2 C(x,t)}{\partial x^2} - \lambda_{Rn} C(x,t) + f, \quad \text{for } 0 < x < d, \quad t > 0 \tag{1}$$

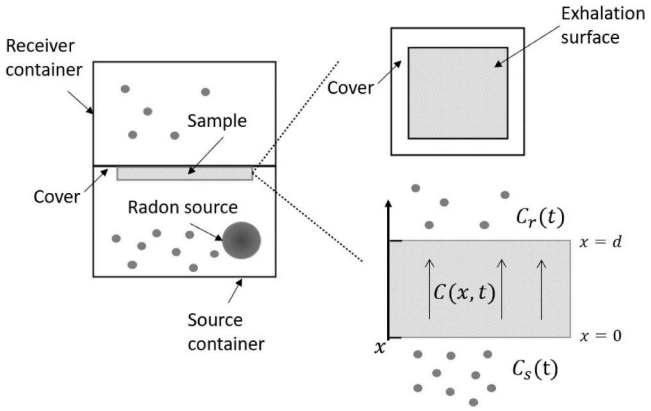

Fig. 1. Experimental set-up for the determination of the radon diffusion coefficient. $x(m)$: position along the thickness of the material. d (m): thickness of the material. $C(x,\ t)$ $(Bq\ \ m^{-3})$: radon concentration in the material. $C_s(t)$ $(Bq\ \ m^{-3})$ and $C_r(t)$ $(Bq\ \ m^{-3})$: radon concentrations at the source and receiver container respectively.

- t: time (s)
- x: position along the thickness of the material (m)
- $C(x,t)$: radon concentration in the porous space of the material $(Bq\ m^{-3})$
- D: radon diffusion coefficient $(m^2\ s^{-1})$
- λ_{Rn}: radon decay constant (s^{-1})
- f: source term for the generation of radon from the material $(Bq\ m^{-3}\ s^{-1})$
- d: thickness of the material (m)

In summary, Eq. (1) is a transient, one-dimensional equation with a diffusion term given by Fick's law, a sink term given by radon decay and a source term from the generation of radon in the material. For the samples studied in this work, the generation of radon from the material is considered null but is a term that can be included with the developed code.

Eq. (1) has the following boundary and initial conditions [45]:

$$-D\frac{\partial C(x,t)}{\partial x} = h\left(C_{x_0} - C_s\right), \quad \text{for } x = 0, \quad \forall t \tag{2}$$

$$-D\frac{\partial C(x,t)}{\partial x} = h\left(C_{x_d} - C_r\right), \quad \text{for } x = d, \quad \forall t \tag{3}$$

$$C(x,t) = C_0(x), \quad \text{for } t = 0, \quad 0 < x < d \tag{4}$$

- h: radon transfer coefficient $(m\,s^{-1})$ [56]
- C_{x_0}: radon concentration at $x = 0$, the contact point with the source container$(Bq\ m^{-3})$
- C_{x_d}: radon concentration at $x = d$, the contact point with the receiver container$(Bq\ m^{-3})$
- $C_s(t)$: radon concentration in the volume of the source container $(Bq\ m^{-3})$
- $C_r(t)$: radon concentration in the volume of the receiver container $(Bq\ m^{-3})$
- $C_0(x)$: initial radon concentration in the material $(Bq\ m^{-3})$

Eqs. (2) and (3) are boundaries conditions that reflects the gradient in concentration of radon with a transfer constant h, and how the transport at the top and bottom layers of the materials are determined by the concentrations to which the material is exposed at each side. The value of h was set to $0.1\,m\,s^{-1}$, which is the value used in [44]. A sensitivity study was carried out to determine the influence of changes in h, but different values were used and no significant difference in the result was found up to 5 orders of magnitude.

A higher concentration in the receiver chamber would reduce the radon concentration gradient and hence the flux through the top layer of the material. Furthermore, the concentration in the source container is expected to be much higher than in the material, provided that the material's own radon generation is negligible, transporting radon from the source container, $C_s(t)$, through the material, $C(x,t)$, up to the receiver container, $C_r(t)$.

Eq. (4) reflects the initial concentration of radon in the material. If it was previously exposed to a radon concentration, the initial concentration can be found by solving for the stationary state of Eq. (1).

2.1.2. Radon accumulation at receiver container

The concentration at the source container is known from measurements and the concentration at the receiver container follows a known accumulation equation for each time step [45,57,58]:

$$C_{r,i} = C_{r,i-1}e^{-\lambda_{ef}\Delta t} + \frac{E_{i-1}S}{V\lambda_{ef}}\left(1 - e^{-\lambda_{ef}\Delta t}\right), \tag{5}$$

- $C_{r,i}$: radon concentration in the receiver container at time step i $(Bq\ m^{-3})$
- $C_{r,i-1}$: radon concentration in the receiver container at time step $i-1$ $(Bq\ m^{-3})$
- λ_{ef}: effective decay constant (s^{-1})
- Δt: time difference between time step i and $i-1$ (s)
- E_{i-1}: radon exhalation rate from the material to the receiver container at time step $i-1$ $(Bq\ m^{-2}\ s^{-1})$
- V: accumulation volume, in this case the volume of the receiver container (m^3)
- S: exhalation surface, in this case the surface of the material that is exposed to the receiver container (m^2)

$$E_{i-1} = h\left(C_{x_d,i-1} - C_{r,i-1}\right), \tag{6}$$

- $C_{x_d,i-1}$: radon concentration in the material at the position in contact with the receiver container at time step $i-1$ $(Bq\ m^{-3})$

$$\lambda_{ef} = \lambda_{Rn} + \lambda_b + \lambda_l, \tag{7}$$

- λ_l: leakage constant, for the leaks in the experimental set up (s^{-1})
- λ_b: bound exhalation constant, for the reduction of the exhalation as the radon concentration increases (s^{-1})

Eqs. (5) and (6) show that the radon concentrations in the material and in the receiver container are dependent on each other through the exhalation rate. The effective decay constant is obtained by fitting the experimental accumulation curve in the receiver container [57,58].

Using the experimental measurement in the source and receiver containers together with Eq. (5) and the numerical solution of Eq. (1), the developed algorithm will search for the best value of the radon diffusion coefficient.

2.2. Radon diffusion coefficient search algorithm

The developed code solves Eq. (1) by applying the finite element method (FEM) in a one-dimensional mesh along the x-axis, using the standard Galerkin approach and the trapezoidal rule for the discretisation in space and time respectively [59,60]. A system of linear algebraic equations is obtained, with the nodal concentrations as the unknown values, and solved using the standard Gaussian elimination method.

The steps taken by the algorithm to solve the equations while testing a D value are as follows. First, if the material was placed on top of the source container before the start of the measurements to have an initial radon concentration, i.e. to saturate the material with radon, the initial condition on the material, Eq. (4), has to be calculated. This is done by solving Eq. (1) with the FEM in the steady state and using the first measured concentrations at the boundary conditions, Eq. (2) and (3). If not, the initial concentration is set to zero. Once it has the initial conditions, it stars to iterate in time. It first calculates the value of the concentration in the receiver container in the first time step with Eq. (5) using the data from the previous time step, from the initial conditions in this case. Then, it solves Eq. (1) with the FEM using the calculated concentration in the receiver container in Eq. (2) and the measured concentration in the source container in Eq. (3) for that time step. The same is then done for the next iteration until it reaches the last time step. Another option, if the sample was left beforehand to saturate but measurements were taken during this period, is to also iterate during this time but force the concentration in the receiver container to zero. All of this can be chosen by the user when applying the algorithm.

The best value for the radon diffusion coefficient can be found by solving Eq. (1) for different values of D and comparing the radon concentrations obtained by Eq. (5) with the experimental measurements. The algorithm starts with two initial values of D, introduced by the

user, then generates the radon concentration for these two cases and compares them with the experimental data by using the mean absolute error, *MAE*. After the comparison, it selects the *D* value for which the differences between the experimental and calculated concentrations are lower, meaning a lower *MAE*. Then it generates a new value to perform a new iteration with two other values of *D*, the selected one and the generated one. This new value is generated in the direction indicated by another statistical parameter, the *BIAS*, and the step taken is half the difference between the two values previously compared. All this is repeated until one of the conditions applied is reached. The parameters mentioned and the possible conditions are defined below.

The steps taken by the script are explained below in more detailed and are shown in the flow chart in Fig. 2.

With each pair of *D* values, the script compares the predicted results to the experimental measurement using the *MAE*, which is defined as:

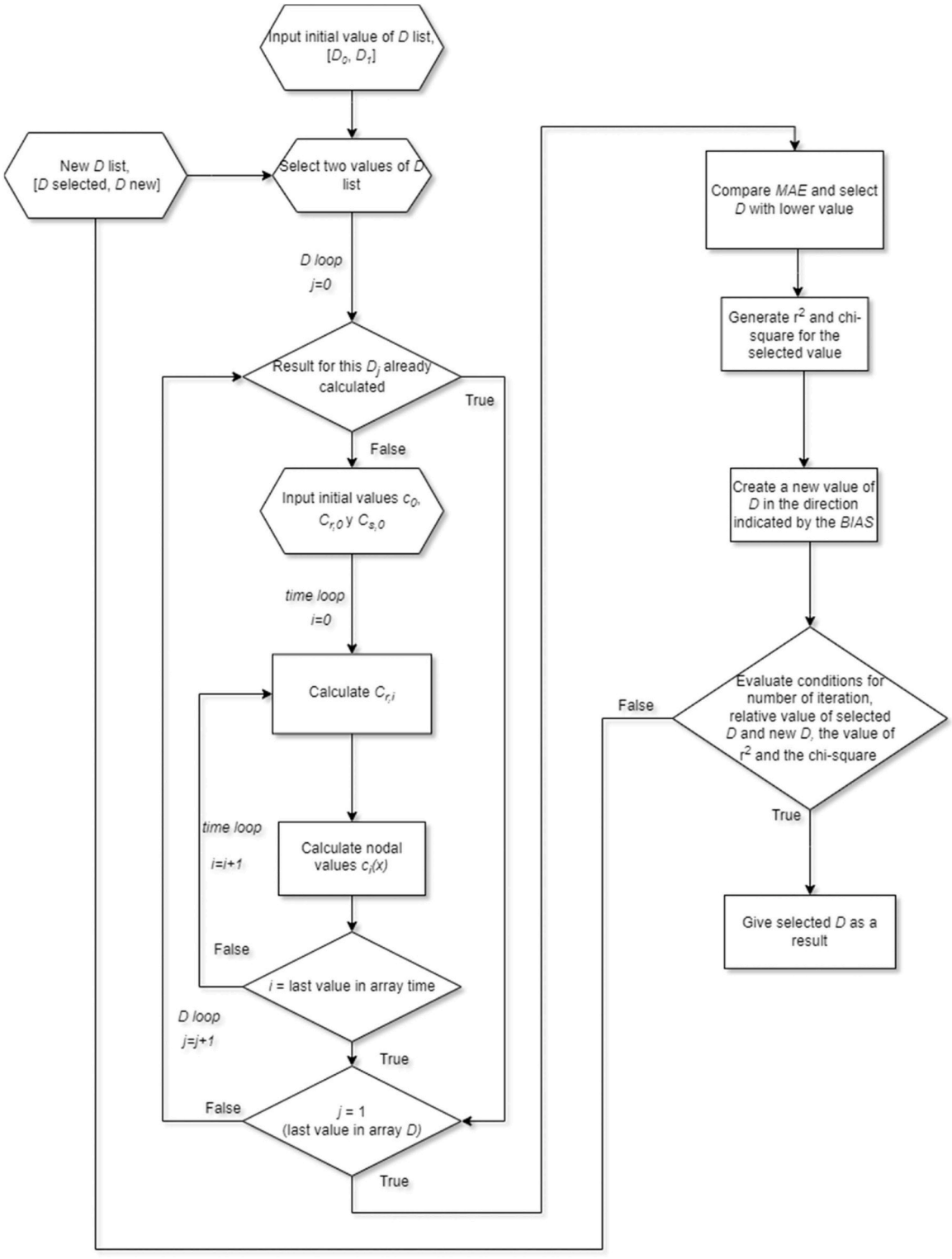

Fig. 2. Algorithm flow chart.

$$MAE = \frac{1}{N}\sum_{i=1}^{N}|C_{r,i}^{p} - C_{r,i}^{e}|, \tag{8}$$

- N: the total number of time steps
- $C_{r,i}^{p}$: radon concentration in the receiver container predicted by the code at time step i with Eq. (5) ($Bq\ m^{-3}$)
- $C_{r,i}^{e}$: radon concentration in the receiver container at time step i experimentally measured ($Bq\ m^{-3}$)

Once the best value of D between the two is selected, another statistical parameter, the *BIAS*, is used to know the direction in which D should change to get closer to the optimal value. Essentially, this parameter determines if the tested value for D was overestimated or underestimated and deduces if the next value should be higher or lower than the previous one. The *BIAS* is defined as:

$$BIAS = \frac{1}{N}\sum_{i=1}^{N}(C_{r,i}^{p} - C_{r,i}^{e}). \tag{9}$$

A new value for D is then generated by taking a step from the selected D equal to half the difference between the two previously compared values in the direction indicated by the *BIAS*. This step size ensures that the algorithm always converges after successive iterations, rather than fluctuating around an asymptotic value. The comparison and selection of a D value is then performed again, this time between the selected and the generated value.

In the developed code 4 types of conditions to stop the iterations and return the last selected value of D are possible to apply, and are as follows:

1. When the number of iterations reaches a predefined value. The default value is 100 iterations. This condition prevents the algorithm from getting trapped in loop cases and never reaching completion.
2. When the relative difference between the new generated value of the D and the selected one, defined as:

$$RD(D_{new}, D_{selected}) = \frac{|D_{selected} - D_{new}|}{D_{selected}} \bullet 100, \tag{10}$$

   is less than a selected value, to study if the improvement in D is significant. The default value is 10%. This condition is based on the idea of terminating the iteration process if it has reached a value that accurately reproduces the experimental measurements and the new test values are not significantly improving the outcome.
3. When the value of χ^2, defined as [61,62]:

$$\chi^2 = (N-1)\frac{\sigma_{ext}^2}{\sigma_{\text{int}}^2}, \tag{11}$$

   o σ_{int} : internal uncertainty ($Bq\ m^{-3}$)
   o σ_{ext} : external uncertainty ($Bq\ m^{-3}$)

$$\sigma_{\text{int}} = \frac{1}{\sqrt{\sum_{i=1}^{N}\left(\sigma(C_{r,i}^{e})\right)^{-2}}}, \tag{12}$$

   o $\sigma(C_{r,i}^{e})$: the uncertainty of the measurement $C_{r,i}^{e}$ ($Bq\ m^{-3}$)

$$\sigma_{ext} = \sqrt{\frac{\sum_{i=1}^{N}\left(C_{r,i}^{p} - C_{r,i}^{e}\right)^{2}\left(\sigma(C_{r,i}^{e})\right)^{-2}}{(N-1)\sum_{i=1}^{N}\left(\sigma(C_{r,i}^{e})\right)^{-2}}}. \tag{13}$$

   is less than a critical value obtained for a significance level. The default value is a significance level of 1%.
4. When the value of the coefficient of determination, r^2, defined as:

$$r^2 = 1 - \frac{\sum_i\left(C_{r,i}^{e} - C_{r,i}^{p}\right)^2}{\sum_i\left(C_{r,i}^{e} - \overline{C}_{r}^{e}\right)^2}, \tag{14}$$

   o $\overline{C}_{r}^{e}$: mean radon concentration in the receiver container experimentally measured ($Bq\ m^{-3}$)

   is higher than a selected value. The default value is 0.95. This condition checks if the generated curve is a good fit of the experimental data.

In summary, the code will minimise the parameter *MAE* in order to get closer to a value of D that better fits the experimental measurements, until it considers that further iteration will not lead to better results.

3. Experimental set-up and materials

3.1. Experimental set-up

The experimental set-up consists of two accumulation chambers of 2.4 L each, a perforated cover, that fits between the two chambers and where the problem material is placed, a radon source, and two radon detectors, a RTM 1688-2 (SARAD) and a RAD7 (DURRIDGE) (Fig. 3). To avoid systematic differences in the measurements, the detectors were compared against each other using a reference soil [58].

The accumulation chambers are of reduced size and made of polypropylene, although iron chambers are normally used. The cover is made of the same material of the chamber, as it is the actual cover of the chamber where a perforation was made. The leaks of the chambers were taken into account by calculating the effective decay constant through the fitting of the measurement data for each experiment. The sealing of the experimental set-up, of the chambers with the different sides of the cover and of the sample with the cover, was done by using acrylic filler. The problem material is attached to the cover and the acrylic filler ensures that the material is held in place and secure (Figs. 1 and 3). Both the chambers material and the filler were tested to assured radon leaks and to verify its suitability for the ISO application.

To reach a higher concentration in the receiver container at the time of the measurements, the sample is left to saturate with radon beforehand. This is done by leaving the set-up of radon source, source container, cover, and sample to accumulate for one week so when the measurements start the concentrations in the receiver container will evolve faster and will be high enough to avoid low precision when measuring the radon concentration. In consequence, the initial concentration in the material will not be null and will be calculated by the algorithm applying the corresponding boundary conditions. After a week, the receiver container is placed on top of the cover and the actual measurements begin. This accumulation step makes the methodology scalable as it allows to have different samples getting ready while only using two detectors for the actual measurements.

3.2. Materials

The methodology was applied to two membranes provided by BMI Group (https://www.bmigroup.com/es/) and some typical construction materials (Fig. 4). The characteristics of the samples are described in Table 1. These materials have been selected to cover a range of thicknesses and compositions. Also, for some of the materials, their radon diffusion coefficient has been previously measured in the literature and we can use this as a reference to verify the results provided by the code.

During this work, 49 different experiments were compared for a variety of materials, with thicknesses ranging from 0.4 to 20.5 mm,

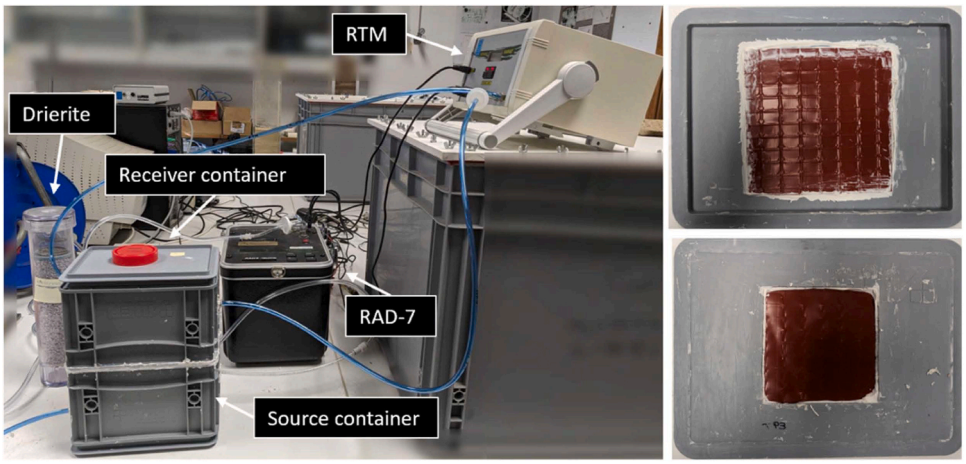

Fig. 3. Experimental set-up for the radon diffusion coefficient methodology and the cover with a sample placed in it.

Fig. 4. Picture of the measured samples.

radon diffusion coefficient from 10^{-7} to 10^{-12} m^2 s^{-1} and measurements ranging from 18 to 258 hours. Also, a minimum of two different measurements for each sample were done, allowing the calculation of an uncertainty. For the commercial membranes, since two of each type of membrane were provided, the measurements were repeated four times, two in each parallel sample.

4. Results and discussion

4.1. Stop conditions and convergence evaluation

As it was explained, there are different stop conditions that can be applied to stop the iterations and obtain a final result of D. Up to 9 different conditions were tested:

1. If the $RD(D_{new}, D_{selected})$ is less than:
   a. (condition C1).

Table 1
Description of the measured samples.

Code	Description	Thickness (*mm*)
M1	Reinforced double layer low-density polyethylene and polyester[a] membrane	0.4
M2	Elastomer modified bitumen[b] membrane	3.3
M3	Portland cement paste	10.8
M4	Marble	20.5
M5	Marble + Porcelain	9.8
M6	Mud brick	19.4
M7	Red paste with enamel	6.6
M8	Handmade ceramics	12.5
M9	Slate	7.1
M10	Hydraulic	17.5

[a] Commercial name Monarflex RMB 400.
[b] Commercial name Polibater combi 48.

   b. (condition C2).
   c. (condition C3)
2. If the χ^2 for the selected D is less than the critical value of χ^2 for a:
   a. level of significance (condition C4).
   b. level of significance (condition C5).
   c. level of significance (condition C6).
3. If the r^2 for the selected D is greater than:
   a. 0.8 (condition C7).
   b. 0.9 (condition C8).
   c. 0.95 (condition C9).

To study the stop conditions, they were applied to 49 different experiments of varying duration and on a variety of materials with different thicknesses and radon diffusion coefficients.

Fig. 5(a), (b) and (c) represent, for all the experiments, the relative difference between the D for each iteration and the D at iteration 50, $RD(D,D_{50})$, the relative difference between the χ^2 for each iteration and the χ^2 at iteration 50, $RD(\chi^2, \chi^2_{50})$, and the r^2 for each iteration, respectively.

The search algorithm was instructed to stop after 50 iterations to compare the results obtained for each of the conditions with the value of D to which the code converges, so the convergence of the parameters can be studied.

For these experiments, a wide range was chosen for the initial D values, more specifically from $10^{-6}\ m^2\ s^{-1}$ to $10^{-13}\ m^2\ s^{-1}$. This would ensure that the initial range would contain all possible values known from the literature and exemplifies a worst case where no prior knowledge of the diffusion coefficient of the material is known. These values are relevant since how close the initial given values are to the best fitting value will determine how fast the algorithm converges to a value of D. This is the main difference between the behaviour of the curves in Fig. 5. In some cases, if one of the initial values is significantly closer than the other, the code will choose one of the initial values of D for several iterations, and the results do not start to show improvements until after 10 or even 15 iterations.

In general, most parameters in Fig. 5 show a consistent improvement as the number of iterations increases. This is the case for $RD(D,D_{50})$, and for r^2. Regarding the latter, there are 3 instances where the parameter never goes above 0.8. This shows that in those cases where the experimental values of the radon concentration have a higher dispersion, this parameter might not reach values closer to 1 since the experimental and calculated values will never converge. However, most of the experiments, 46 out 49, reach higher values of r^2. Lastly, the parameter χ^2 does not decrease systematically in some experiments. Instead, it can increase for some iterations and then decrease again to the convergence value. This happens because χ^2 is not the parameter we are minimising, but it eventually stabilises. In all cases, the parameters converge or effectively

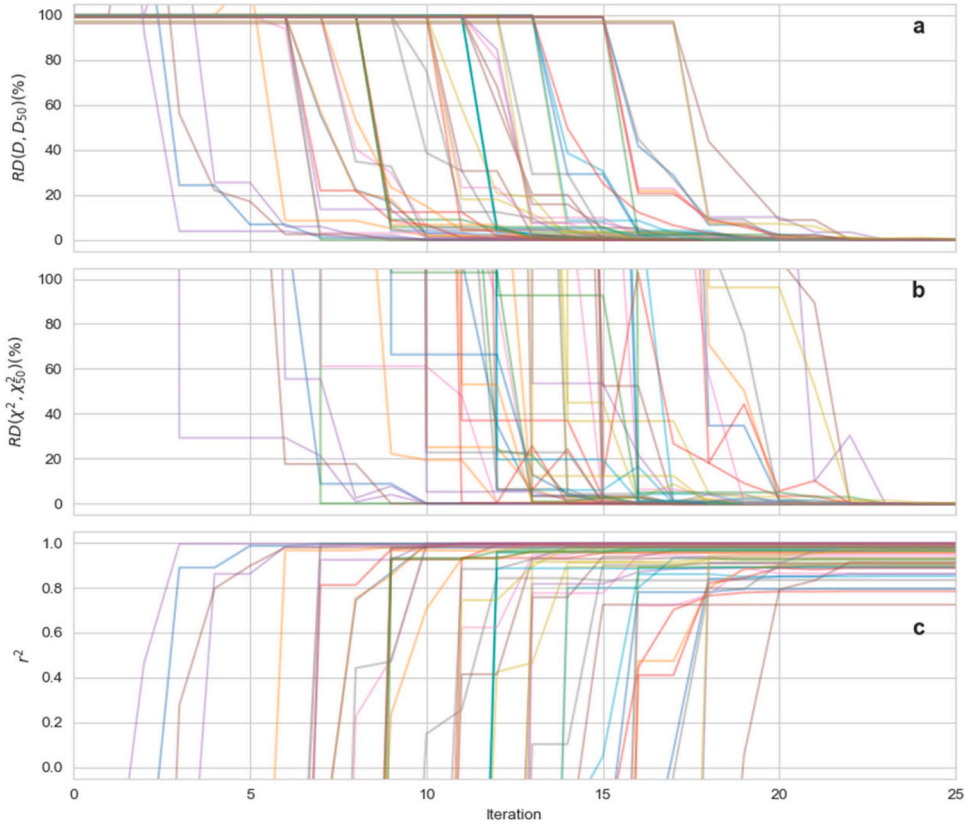

Fig. 5. (a) Relative difference between the D of the iteration with the D at iteration 50, (b) relative difference between the χ^2 of the iteration with the χ^2 at iteration 50, and (c) r^2 of the iteration, for the 49 experiments.

do not change, before 25 iterations.

Table 2 shows the different thresholds applied for the parameters to study the stop conditions applied to the 49 experiments. Firstly, the percentage of experiments that reached the condition is shown to know how restrictive the condition is. Secondly, the average relative difference of all the experiments, $RD(D, D_{50})$, is shown to indicate how close from the asymptotic value each condition is, i.e., how accurate is the result with respect D_{50}. Thirdly, the range is also shown to indicate the dispersion of the values reached by each condition. Lastly, the last parameter is how many iterations on average was need, showing which condition is faster.

The results in Table 2 show that conditions C1, C2 and C3, which all refer to $RD(D_{new}, D_{selected})$, are reached by all the experiments, making this type of condition the more stable one as the algorithm will always reach a result. The more restrictive this condition gets, the closer the result is to the value at D_{50}, i.e., the $RD(D, D_{50})$ mean is lower, but it takes more iterations. The value of D obtained with condition C3 is the closest, between the 9 conditions, to the converge value, with a $RD(D, D_{50})$ mean of 0.1%. It is also the one that takes the longest, as the mean number of iterations is the highest, 18. This shows that a more accurate result takes more time.

For the conditions C4, C5 and C6, which all refer to χ^2, the results are similar, but the number of experiments that reach the condition show that, as expected, a lower level of significance allows more experiments to reach the condition. The specific percentage ranges from 47% (significance level of 10%) to a 65% (significance level of 1%). Looking at the percentage of experiments in Table 2, we can see that these are the more restrictive conditions.

Conditions C7, C8 and C9 are the fastest, as their mean number of iterations are the lowest, but, to get a result close to the convergence value, the most restrictive of the 3 should be applied. They also have the higher dispersion among all conditions.

Additionally, these 9 conditions were applied to the same experiment in order to better study the relationship between accuracy and execution time by comparing them in one specific situation. The experiment chosen was the 1st one made on sample M1, since in this case the 9 conditions were reached.

Table 3 shows the different parameters used to study the conditions performance. With the execution time and the number of iterations we compare how fast the conditions are, and with D and $RD(D, D_{50})$ we compare the results and how close they are to the convergence value.

Table 3 shows the results of applying these 9 conditions to the same experiment. The condition that takes the longest is C3, with 25 iterations and 3.9 minutes, but this longer time results in the obtained D being the same as the convergence value of D. For the rest of the conditions, except C7 and C8, the results are almost the same as the convergence value of D, with only a relative difference of , taking a few seconds less. Although this difference in time may not be significant for a single experiment it can add up when experiments are run systematically.

The stop conditions can be combined, and the code will stop when one of them is reached. A good compromise between time and a good result is to use C2, C4 and C9, as they are all close enough to the D value of convergence, with a relative difference of only a , and in the case that conditions C4 and C9 are met, the computation time is reduced.

4.2. Detection limit

In order to study what is the minimum D that can be determined with the methodology, the minimum detectable diffusion coefficient, MDDC, data for the radon concentration measurements in the receiver container, C_r^e, was simulated. The simulated accumulation concentration was chosen to saturate at 6 $Bq\ m^{-3}$, since this is the detection limit calculated for the RTM detector with 6 counts and a cycle of 1 hour, and to have a λ_{ef} of $10^{-5}\ s^{-1}$, which is a normal value calculated in the experiments. The MDDC values were calculated with the code for a range of sample thickness from 0.01 cm to 1 cm and a range of concentrations in the source container from 10 $kBq\ m^{-3}$ to 1 $MBq\ m^{-3}$.

Fig. 6 shows the representation of the MDDC calculated by the algorithm as a function of the thickness of the material with different curves for the different concentrations in the source container (Fig. 6 (a)), and as a function of the source concentration for 3 values of the thickness (Fig. 6(b)).

As expected, for each of the source concentration curves (Fig. 6(a)), the resulting MDDC increases with the thickness of the material. This is because a higher thickness makes the diffusion of radon into the receiver container more difficult, and in consequence there is a higher MDDC for the same receiver concentration.

Also, for each thickness, the MDDC is lower for a higher concentration in the source container, this can be seen more clearly in Fig. 6(b). A higher concentration in the source container for the same concentration in the receiver container results in a lower MDDC as less radon is being able to diffuse through the material.

For the tested cases, the minimum MDDC obtained was a value of $4.54 \bullet 10^{-15}\ m^2\ s^{-1}$ for a thickness of 0.01 cm and a concentration in the source container of 1 $MBq\ m^{-3}$, and the maximum value was of $4.59 \bullet 10^{-11}\ m^2\ s^{-1}$ for a thickness of 1 cm and a source concentration of 10 $kBq\ m^{-3}$.

The minimum D that can be calculated with the methodology depends on the thickness of the sample, the concentration in the source container and the detection limit of the detector measuring in the receiver container, and curves for different cases can be calculated using the developed algorithm.

4.3. Validation and application

In the case of the radon diffusion coefficient, there is no Certified Reference Material with an established value of D that can be measured to validate the algorithm and methodology. For this reason, an internal validation was firstly carried out by repeating the experiments for each sample and an external validation by comparison with the literature.

The methodology for the measurement of the radon diffusion coef-

Table 2
Comparison of different conditions to stop the code for 49 tested experiments. Percentage: percentage of experiments that reached the condition. $RD(D, D_{50})$ mean: mean of the relative differences between the result D for the condition and the one at iteration 50. $RD(D,\ D_{50})$ range: range of values of the relative difference. Mean iterations: average of the number of iterations.

Nomenclature	Condition	Percentage (%)	$RD(D, D_{50})$ mean (%)	$RD(D, D_{50})$ range (%)	Mean iterations
C1	$RD(D_{new}, D_{selected}) \leq 20\%$	100	4.3	0 – 9.6	13
C2	$RD(D_{new}, D_{selected}) \leq 10\%$	100	1.9	0 – 5.2	14
C3	$RD(D_{new}, D_{selected}) \leq 1\%$	100	0.1	0 – 0.5	18
C4	$\chi^2 \leq \chi^2_{1-0.01}$	65	2.8	0 – 9.3	15
C5	$\chi^2 \leq \chi^2_{1-0.05}$	57	2.3	0 – 8.6	15
C6	$\chi^2 \leq \chi^2_{1-0.1}$	47	2.2	0 – 7.6	16
C7	$r^2 \geq 0.8$	94	7.6	0 – 25.5	12
C8	$r^2 \geq 0.9$	78	4.6	0 – 13.5	12
C9	$r^2 \geq 0.95$	57	3.3	0 – 8.6	11

Table 3
Comparison of different conditions to stop the code for the 1st experiment on sample M1. The D obtained for iteration 50 was $D_{50} = 3.56 \bullet 10^{-12}\ m^2\ s^{-1}$. $RD(D,D_{50})$: relative differences between the result D for the condition and the one at iteration 50.

Nomenclature	Condition	Execution time (min)	Iterations	$D(m^2\ s^{-1}) \bullet 10^{-12}$	$RD(D,D_{50})$ (%)
C1	$RD(D_{new}, D_{selected}) \leq 20\%$	3.3	21	3.44	3
C2	$RD(D_{new}, D_{selected}) \leq 10\%$	3.5	22	3.68	3
C3	$RD(D_{new}, D_{selected}) \leq 1\%$	3.9	25	3.56	0
C4	$\chi^2 \leq \chi^2_{1-0.01}$	3.3	21	3.44	3
C5	$\chi^2 \leq \chi^2_{1-0.05}$	3.3	21	3.44	3
C6	$\chi^2 \leq \chi^2_{1-0.1}$	3.3	21	3.44	3
C7	$r^2 \geq 0.8$	2.9	18	3.92	10
C8	$r^2 \geq 0.9$	2.8	18	3.92	10
C9	$r^2 \geq 0.95$	3.3	21	3.44	3

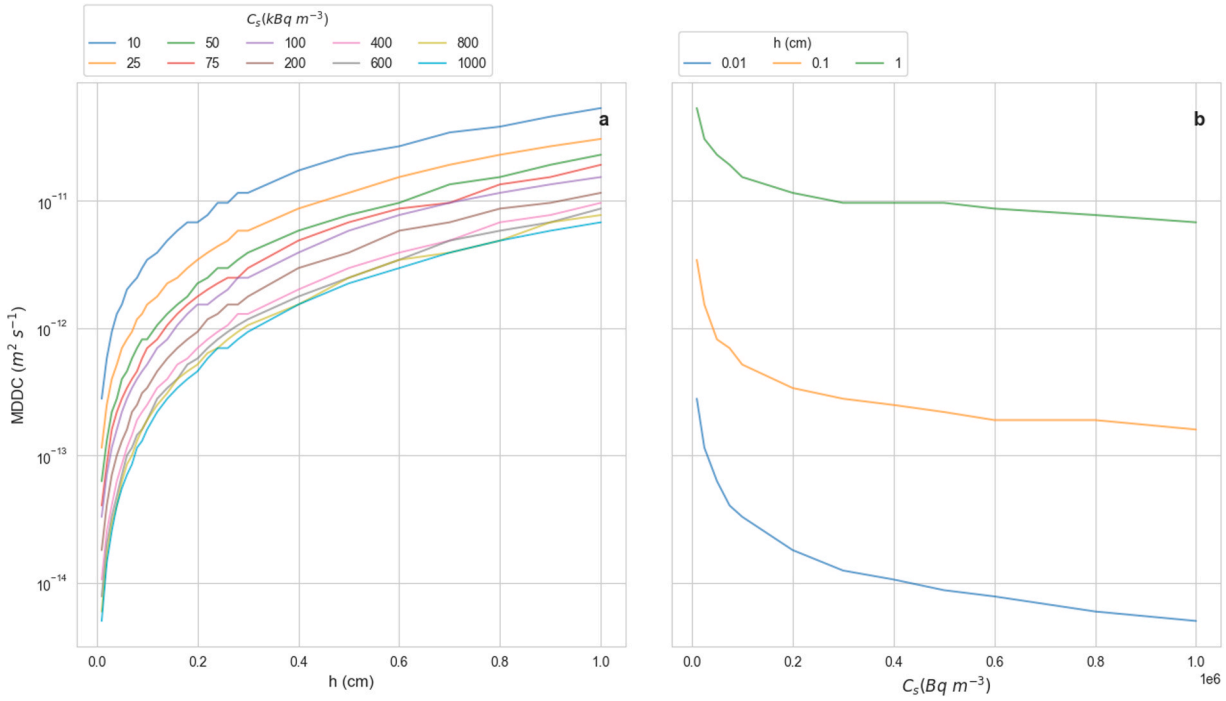

Fig. 6. Minimum detectable diffusion coefficient, MDDC, (a) with the thickness of the sample for different concentrations in the source container, and (b) with the concentration in the source container for 3 different thickness of the sample. Y-axis scale is logarithmic.

ficient was applied to 10 different samples. The results for D were obtained using the developed code and applying conditions C2, C4 and C9. The samples were left beforehand to saturate in all cases. The measurements of the radon concentration in the source and receiver container, alongside the radon concentration predicted by the algorithm for the fitting D, are shown in Fig. 7 for the 3rd experiment on the sample M1 (Fig. 7(a)) and for the 1st experiment on the sample M2 (Fig. 7(b)).

The evolution of the concentration in the receiver container increases as radon is transported from the source container and saturates to a value over time. For the source container, the concentration changes as the conditions change from the chamber being closed to being in a close circuit with the equipment, and from the sample being exposed to the air to then being exposed to the receiver container. This will cause the radon concentration to change and reach a new equilibrium. Also, in some cases, the concentration in the source container is not as high as the ones recommended by the ISO [44], within 1 $MBq\ m^{-3}$ to 100 $MBq\ m^{-3}$, but still the radon diffusion coefficient is estimated correctly with our experimental set-up.

For the two experiments shown in Fig. 1 a solution was found in less than 3 minutes, given as initial values $10^{-6}\ m^2\ s^{-1}$ and $10^{-13}\ m^2\ s^{-1}$. The D value chosen by the algorithm predicts very well the evolution of the concentration at the receiver container for samples M1 and M2. This is also reflected in the value of the r^2 calculated between the predicted and experimental concentrations, which is of 0.90 for sample M1 (Fig. 7 (a)) and of 0.96 for sample M2 (Fig. 7(b)). The good reproduction of the accumulation over time further confirmation of the ability of the algorithm to reproduce the physical conditions of the experimental set-up.

Fig. 8 shows the D obtained with the search algorithm for the different experiments taken on the samples and the calculated mean value with his uncertainty, calculated with the standard deviation of the mean.

When the experiment was repeated for each of the samples, the results obtained were always of the same order of magnitude and, in general, the values obtained for each sample were similar, showing the consistency of the methodology, that is, showing a good internal validation. The good repeatability of the method is important in order to have a standard measurement of this parameter. This is reflected in the relative error shown in Table 4 which was around .

The mean value of D, $\overline{D}$, with his uncertainty, $\sigma_{\overline{D}}$, the relative error between the two, $\epsilon_{\overline{D}}$, and the D values found in the literature for similar samples are shown in Table 4 in order to carry out the external validation of our code and methodology.

The mean value of D and the literature values are also shown in Fig. 9 for comparison.

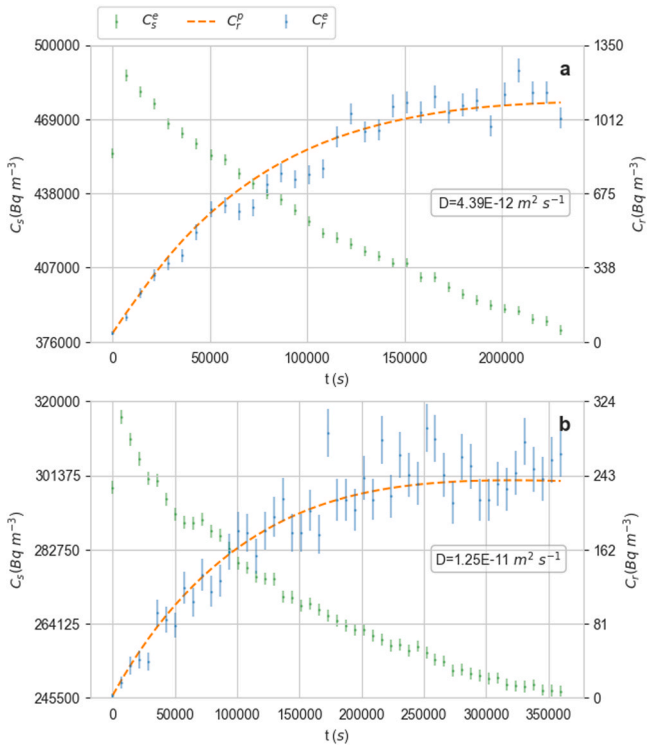

Fig. 7. Concentrations measured in the receiver container, C_r^e and source container, C_s^e, along with the theorical curve obtained with the search algorithm for the final chosen D value, C_r^p, for an experiment (a) on the sample M1 and (b) on the sample M2.

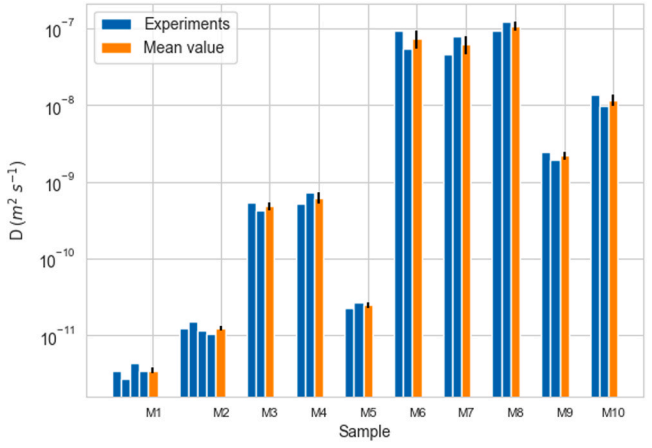

Fig. 8. Radon diffusion coefficient obtained with the search algorithm for the different experiments performed in each of the samples and their mean value. Y-axis scale is logarithmic.

The values obtained for the mean D values agree well with reference ones, considering they are not the same samples, only similar, with the data found in the literature.

M1 and M2 are commercial membranes with a previously measured D value. The result obtained for M1 is very similar to that given in the product data sheet, but not so much for M2. However, in the case of the sample M2, the uncertainty provided in the literature is relatively high (about 50% of relative uncertainty), and when this uncertainty is given at 2 sigma level, the reference D value is of the same order of magnitude as the one obtained in this study.

In the case of the Portland cement mortar, sample M3, the samples found in the literature are of Portland cement with different percentages

Table 4
Final mean D result ($\overline{D}$) for the tested samples with our methodology, with its uncertainty ($\sigma_{\overline{D}}$) and relative error ($\epsilon_{\overline{D}}$), and comparison with the literature.

Code	Material	$\overline{D} \pm \sigma_{\overline{D}}$ $(10^{-10}\ m^2\ s^{-1})$	$\epsilon_{\overline{D}}$ (%)	$D\ (10^{-10}\ m^2\ s^{-1})$ in literature
M1	Monarflex RMB 400	0.035 ± 0.003	9	0.034 ± 0.010[a]
M2	Polibater combi 48	0.125 ± 0.010	8	0.046 ± 0.020[a]
M3	Portland cement paste	4.9 ± 0.6	12	$5.8 - 420$[b]
M4	Marble	6.3 ± 1.1	17	9.9 ± 0.3[c]
M5	Marble + Porcelain	0.249 ± 0.019	8	-
M6	Mud brick	740 ± 200	27	$1000 - 5000$[d]
M7	Red paste with enamel	630 ± 160	25	3500 ± 500[e]
M8	Handmade ceramics	1090 ± 160	15	
M9	Slate	22.0 ± 2.4	11	-
M10	Hydraulic	117 ± 20	17	-

[a] BMI Group
[b] [63–65],
[c] [66],
[d] [67],
[e] [46].

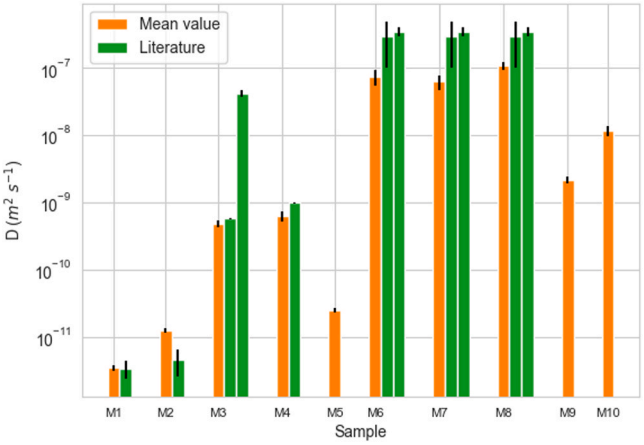

Fig. 9. Mean radon diffusion coefficient for each of the samples and comparison with the literature.

of silica fume and rice husk ash [63–65]. There are many factors in the production process, such as the additive percentages, water/cement ratios or curing days, that can affect the properties of the material, like the density, the porosity, or the compression stress, and consequently the resulting radon diffusion coefficient. It is therefore a good result to have found a similar order of magnitude for D.

For the marble, sample M4, only one result was found in the literature [66]. The samples are not the same ones but the order of magnitude of the result for the sample M4 is the same as the literature. Stacking another material on top of the marble, the porcelain in sample M5, results in a lower value, meaning that the porcelain has a smaller D.

Samples M6, mud brick, M7, red paste with enamel, and M8, handmade ceramics, are all made from the same type of material, clay, but are treated differently in the manufacturing process. A value was found in the literature for clay bricks [46,67] and although the samples are not the same, only the type of material, the order of magnitude of D aggress well. Of the clay materials, the red paste is the one with the lower D, probably for the addition of the enamel.

The samples of slate, M9, and hydraulic, M10, were not found in the literature but a value of $(2.20 \pm 0.24) \bullet 10^{-9}\ m^2\ s^{-1}$, and

$(1.17 \pm 0.20) \bullet 10^{-8}\ m^2\ s^{-1}$, respectively, were found.

5. Conclusions

The main result of this work is the open-source algorithm that was developed and tested to complement the methodology established by ISO 11665-13 [44] for the measurement of the radon diffusion coefficient in a material. It was applied to a variety of experiments to study the convergence of the different statistical parameters used by the code and the different conditions that can be applied with them to stop the algorithm.

The main conclusions were the following:

1. The statistical parameters used in the developed algorithm converged in a few iterations for the tested experiments, less than 25, and the selection of more restrictive conditions lead to better fitting results at the cost of more computation time.
2. The MDDC can be calculated for different conditions using the developed code, depending on the detection limit of the detector measuring in the receiver container, the radon source used and the thickness of the sample.
3. The radon diffusion coefficient of different materials was measured. When the measurements were repeated on the same sample the results obtained were similar, showing good repeatability. The results agreed with those found in the literature, at least in magnitude order, as the samples are not the same ones. There are also measurements for materials not found in previous literature.

In summary, the developed code was verified satisfactorily and made available for their easy use, making this methodology easy to replicate and apply.

CRediT authorship contribution statement

E. Castaño-Casco: Conceptualization, Investigation, Methodology, Software, Formal analysis, Data curation, Validation, Visualization, Writing – review & editing, Writing – original draft. **I. Gutiérrez-Álvarez:** Conceptualization, Investigation, Methodology, Resources, Software, Visualization, Writing – review & editing. **A. Barba-Lobo:** Conceptualization, Investigation, Methodology, Writing – review & editing. **J.P. Bolívar:** Conceptualization, Methodology, Resources, Funding acquisition, Project administration, Supervision, Writing – review & editing.

Declaration of Competing Interest

The authors declare that they have no known competing financial interests or personal relationships that could have appeared to influence the work reported in this paper.

Data availability

Data will be made available on request.

Acknowledgements

This research was partially funded by the Nuclear Safety Council (CSN) by the project “Radon exhalation from building materials; Radiological impact and corrective measures (EXRADON)” (Ref.: PR-047-2021) and the project funded by the Spanish Ministry of Science, Innovation and Universities’ Research Agency “Development and optimization of a process for removing natural radionuclides in phospho-gypsum leachates (RAD-REMOVE)” (Ref.: PID2020-116461RB-C21).

References

[1] G. Dubois, An Overview of Radon Surveys in Europe, Publications Office, 2005.
[2] J.E. Martín, Naturally occurring radiation and radioactivity, in: Physics for Radiation Protection, John Wiley & Sons, Ltd, 2013, pp. 197–243, https://doi.org/10.1002/9783527667062.ch6.
[3] R.C. Ramola, M. Prasad, T. Kandari, P. Pant, P. Bossew, R. Mishra, S. Tokonami, Dose estimation derived from the exposure to radon, thoron and their progeny in the indoor environment, Sci. Rep. 6 (2016), https://doi.org/10.1038/srep31061.
[4] S. Darby, D. Hill, A. Auvinen, J.M. Barros-Dios, H. Baysson, F. Bochicchio, H. Deo, R. Falk, F. Forastiere, M. Hakama, I. Heid, L. Kreienbrock, M. Kreuzer, F. Lagarde, I. Mäkeläinen, C. Muirhead, W. Oberaigner, G. Pershagen, A. Ruano-Ravina, E. Ruosteenoja, A.Schaffrath Rosario, M. Tirmarche, L. Tomášek, E. Whitley, H. E. Wichmann, R. Doll, Radon in homes and risk of lung cancer: collaborative analysis of individual data from 13 European case-control studies, Br. Med. J. 330 (2005) 223–226, https://doi.org/10.1136/bmj.38308.477650.63.
[5] UNSCEAR, Sources and Effects of Ionizing Radiation: United Nations Scientific Committee on the Effects of Atomic Radiation: UNSCEAR 2008 report to the General Assembly, with scientific annexes., United Nations, 2008. ⟨https://www.unscear.org/⟩ (accessed January 25, 2024).
[6] UNSCEAR, Report to the General Assembly SCIENTIFIC ANNEXES A and B, 2019. ⟨https://www.unscear.org/⟩ (accessed January 25, 2024).
[7] WHO, WHO handbook on indoor radon: a public health perspective, World Health Organization, 2009.
[8] I. Gutiérrez-Álvarez, J. Aroba, J.E. Martín, J.A. Adame, J.P. Bolívar, Use of a fuzzy qualitative model to reanalyze radon relationship with atmospheric variables in a coastal area near a NORM repository, Environ. Technol. Innov. 28 (2022), https://doi.org/10.1016/j.eti.2022.102619.
[9] F. Rezaie, M. Panahi, J. Lee, J. Lee, S. Kim, J. Yoo, S. Lee, Radon potential mapping in Jangsu-gun, South Korea using probabilistic and deep learning algorithms, Environ. Pollut. 292 (2022), https://doi.org/10.1016/j.envpol.2021.118385.
[10] I. Gutiérrez-Álvarez, J.L. Guerrero, J.E. Martín, J.A. Adame, A. Vargas, J.P. Bolívar, Radon transport events associated with the impact of a NORM repository in the SW of Europe, Environ. Pollut. 289 (2021), https://doi.org/10.1016/j.envpol.2021.117963.
[11] N. Ahmad, T. Nasir, J. ur Rehman, H. Ullah, Z. Uddin, Risk assessment of radon in soil collected from chromite mines of Khanozai and Muslim Bagh, Balochistan, Pakistan, Environ. Technol. Innov. 16 (2019), https://doi.org/10.1016/j.eti.2019.100476.
[12] D. Xie, H. Wang, K.J. Kearfott, Z. Liu, S. Mo, Radon dispersion modeling and dose assessment for uranium mine ventilation shaft exhausts under neutral atmospheric stability, J. Environ. Radioact. 129 (2014) 57–62, https://doi.org/10.1016/j.jenvrad.2013.12.003.
[13] M. Fuente, D. Rábago, J. Goggins, I. Fuente, C. Sainz, M. Foley, Radon mitigation by soil depressurisation case study: radon concentration and pressure field extension monitoring in a pilot house in Spain, Sci. Total Environ. 695 (2019), https://doi.org/10.1016/j.scitotenv.2019.133746.
[14] G. López-Abente, O. Núñez, P. Fernández-Navarro, J.M. Barros-Dios, I. Martín-Méndez, A. Bel-Lan, J. Locutura, L. Quindós, C. Sainz, A. Ruano-Ravina, Residential radon and cancer mortality in Galicia, Spain, Sci. Total Environ. 610–611 (2018) 1125–1132, https://doi.org/10.1016/j.scitotenv.2017.08.144.
[15] B.D. Burghele, M. Botoș, S. Beldean-Galea, A. Cucoș, T. Catalina, T. Dicu, G. Dobrei, Floric ă, A. Istrate, A. Lupulescu, M. Moldovan, D. Niț ă, B. Papp, I. Pap, K. Szacsvai, C. Sainz, A. Tunyagi, A. Țenter, Comprehensive survey on radon mitigation and indoor air quality in energy efficient buildings from Romania, Sci. Total Environ. 751 (2021), https://doi.org/10.1016/j.scitotenv.2020.141858.
[16] J. Al-Hubail, D. Al-Azmi, Radiological assessment of indoor radon concentrations and gamma dose rates in secondary school buildings in Kuwait, Constr. Build. Mater. 183 (2018) 1–6, https://doi.org/10.1016/j.conbuildmat.2018.06.152.
[17] J.P. Sá, M.C.M. Alvim-Ferraz, F.G. Martins, S.I.V. Sousa, Application of the low-cost sensing technology for indoor air quality monitoring: a review, Environ. Technol. Innov. 28 (2022), https://doi.org/10.1016/j.eti.2022.102551.
[18] H. Chojer, P.T.B.S. Branco, F.G. Martins, M. Alvim-Ferraz, S.I.V. Sousa, Source identification and mitigation of indoor air pollution using monitoring data – current trends, Environ. Technol. Innov. (2024) 103534, https://doi.org/10.1016/j.eti.2024.103534.
[19] A. Dass, S. Srivastava, G. Chaudhary, Air pollution: a review and analysis using fuzzy techniques in Indian scenario, Environ. Technol. Innov. 22 (2021), https://doi.org/10.1016/j.eti.2021.101441.
[20] EURATOM, Directiva 2013/59/Euratom del Consejo, de 5 de diciembre de 2013, por la que se establecen normas de seguridad básicas para la protección contra los peligros derivados de la exposición a radiaciones ionizantes, y se derogan las Directivas 89/618/Euratom, 90/641/Euratom, 96/29/Euratom, 97/43/Euratom y 2003/122/Euratom, 2013. ⟨https://www.boe.es/⟩ (accessed January 25, 2024).
[21] S.M. Khan, J. Gomes, D.R. Krewski, Radon interventions around the globe: a systematic review, Heliyon 5 (2019), https://doi.org/10.1016/j.heliyon.2019.e01737.
[22] ICRP, Summary of ICRP Recommendations on Radon, 2018. ⟨https://www.icrp.org/⟩ (accessed January 25, 2024).
[23] C. Di Carlo, M. Ampollini, S. Antignani, M. Caprio, C. Carpentieri, B. Caccia, F. Bochicchio, Extreme reverse seasonal variations of indoor radon concentration and possible implications on some measurement protocols and remedial strategies, Environ. Pollut. 327 (2023), https://doi.org/10.1016/j.envpol.2023.121480.
[24] J.C.H. Miles, Temporal variation of radon levels in houses and implications for radon measurement strategies, Radiat. Prot. Dosim. 93 (2001) 369–375, https://doi.org/10.1093/oxfordjournals.rpd.a006449.

[25] IAEA, Protection of the Public Against Exposure Indoors Due to Radon and Other Natural Sources of Radiation, 2015. ⟨http://www-ns.iaea.org/standards/⟩.
[26] B. Collignan, C. Lorkowski, R. Améon, Development of a methodology to characterize radon entry in dwellings, Build. Environ. 57 (2012) 176–183, https://doi.org/10.1016/j.buildenv.2012.05.002.
[27] B.A. Moed, W.W. Nazaroff, Soil as a source of indoor radon: generation, migration, and entry, in: Radon and Its Decay Products in Indoor Air, 1988.
[28] F. Pacheco-Torgal, Indoor radon: an overview on a perennial problem, Build. Environ. 58 (2012) 270–277, https://doi.org/10.1016/j.buildenv.2012.08.004.
[29] T. Tene, C. Vacacela Gomez, G. Tubon Usca, B. Suquillo, S. Bellucci, Measurement of radon exhalation rate from building materials: the case of Highland Region of Ecuador, Constr. Build. Mater. 293 (2021), https://doi.org/10.1016/j.conbuildmat.2021.123282.
[30] A. Tsapalov, K. Kovler, Control of radon emanation at determination of activity concentration index for building materials, Constr. Build. Mater. 160 (2018) 810–817, https://doi.org/10.1016/j.conbuildmat.2017.11.116.
[31] P. Gopalakrishnan, J. Jeyanthi, Importance of radon assessment in indoor environment-a review, Mater. Today Proc. 56 (2022) 1495–1500, https://doi.org/10.1016/j.matpr.2021.12.534.
[32] R.C. Bruno, Sources of indoor radon in houses: a review, J. Air Pollut. Control Assoc. 33 (1983) 105–109, https://doi.org/10.1080/00022470.1983.10465550.
[33] P. Bossew, The radon emanation power of building materials, soils and rocks, Appl. Radiat. Isot. 59 (2003) 389–392, https://doi.org/10.1016/j.apradiso.2003.07.001.
[34] R.M. Harrison, R.E. Hester, Indoor Air Pollution, The Royal Society of Chemistry, 2019, https://doi.org/10.1039/9781788016179.
[35] C. Sabbarese, F. Ambrosino, A. D'Onofrio, V. Roca, Radiological characterization of natural building materials from the Campania region (Southern Italy), Constr. Build. Mater. 268 (2021), https://doi.org/10.1016/j.conbuildmat.2020.121087.
[36] A. Tsapalov, K. Kovler, Revisiting the concept for evaluation of radon protective properties of building insulation materials, Build. Environ. 95 (2016) 182–188, https://doi.org/10.1016/j.buildenv.2015.09.020.
[37] K. Rovenská, M. Jiránek, Radon diffusion coefficient measurement in waterproofings - a review of methods and an analysis of differences in results, Appl. Radiat. Isot. 70 (2012) 802–807, https://doi.org/10.1016/j.apradiso.2012.01.002.
[38] B. Papp, C. Cosma, Methods for measuring radon diffusion parameter of waterproof membranes, J. Radioanal. Nucl. Chem. 303 (2015) 1663–1669, https://doi.org/10.1007/s10967-014-3761-2.
[39] I. Cozmuta, E.R. Van Der Graaf, Methods for measuring diffusion coefficients of radon in building materials, Sci. Total Environ. 272 (2001) 323335, https://doi.org/10.1016/S0048-9697(01)00711-2.
[40] Y. jun Ye, W. hao Wu, S. yang Feng, C. huang Huang, S. Li, Simultaneous determination of the radon diffusion coefficient and the free radon production rate from compact porous emanation media, Build. Environ. 144 (2018) 66–71, https://doi.org/10.1016/j.buildenv.2018.08.015.
[41] W. Arafa, Permeability of radon-222 through some materials, Radiat. Meas. 35 (2002) 207–211, https://doi.org/10.1016/S1350-4487(02)00043-4.
[42] L.S. Quindos, A method for measuring effective radon diffusion coefficients in radon barriers by using modified Lucas cells, Radiat. Meas. 39 (2005) 87–89, https://doi.org/10.1016/j.radmeas.2004.03.029.
[43] A. Tsapalov, L. Gulabyants, M. Livshits, K. Kovler, New method and installation for rapid determination of radon diffusion coefficient in various materials, J. Environ. Radioact. 130 (2014) 7–14, https://doi.org/10.1016/j.jenvrad.2013.12.010.
[44] ISO, Measurement of Radioactivity in the Environment-Air: Radon 222-part 13: Determination of the Diffusion Coefficient in Waterproof Materials: Membrane Two-side Activity Concentration Test Method, 2017. ⟨www.iso.org⟩.
[45] M. Jiranek, Z. Svoboda, Transient radon diffusion through radon-proof membranes: a new technique for more precise determination of the radon diffusion coefficient, Build. Environ. 44 (2009) 1318–1327, https://doi.org/10.1016/j.buildenv.2008.09.017.
[46] S.R. Soniya, S. Abraham, M.U. Khandaker, P.J. Jojo, Investigation of diffusive transport of radon through bricks, Radiat. Phys. Chem. 178 (2021), https://doi.org/10.1016/j.radphyschem.2020.108955.
[47] B. Ruvira, B. García-Fayos, B. Juste, J.M. Arnal, G. Verdú, Experimental estimation of the diffusion coefficient in radon barrier materials based on ISO/TS 11665-13: 2017, Radiat. Phys. Chem. 193 (2022), https://doi.org/10.1016/j.radphyschem.2022.109993.
[48] B. Ruvira, B. García-Fayos, B. Juste, J.M. Arnal, G. Verdú, Determination of the radon diffusion coefficient of thin polyethene and aluminium foils used as single or multilayer configuration barriers, Radiat. Phys. Chem. 200 (2022), https://doi.org/10.1016/j.radphyschem.2022.110329.
[49] P. Szajerski, A. Zimny, Numerical analysis and modeling of two-loop experimental setup for measurements of radon diffusion rate through building and insulation materials, Environ. Pollut. 256 (2020), https://doi.org/10.1016/j.envpol.2019.113393.
[50] J.J. Tejado-Ramos, A. Alvarez-Toral, J. Guillén, M. Carmona-Carmona, F.J. Muñoz-Almaraz, Methodology for assessment of radon diffusion coefficients in membranes, used as radon barriers in construction and refurbishment, Constr. Build. Mater. 414 (2024), https://doi.org/10.1016/j.conbuildmat.2024.134967.
[51] Z. Svoboda, Software Packages TransRn & IterRn, 2008.
[52] V.C. Rogers, K.K. Nielson, R.B. Holt, R. Snoddyt, Radon diffusion coefficients for residential concretes, Health Phys. 67 (1994) 261–265, https://doi.org/10.1097/00004032-199409000-00006.
[53] J. Porstendorfer, G. Buttenveck, A. Reineking, Note Daily Variation of the Radon Concentration Indoors and Outdoors and the Influence of Meteorological Parameters, 1994.
[54] V.C. Rogers, K.K. Nielson, R.B. Holt, Radon diffusion coefficients for aged residential concretes, Health Phys. 68 (1995) 832–834, https://doi.org/10.1097/00004032-199409000-00006.
[55] C. Di Carlo, A. Maiorana, M. Ampollini, S. Antignani, M. Caprio, C. Carpentieri, F. Bochicchio, Models of radon exhalation from building structures: general and case-specific solutions, Sci. Total Environ. 885 (2023), https://doi.org/10.1016/j.scitotenv.2023.163800.
[56] M. Jiranek, Z. Svoboda, Numerical modelling as a tool for optimisation of sub-slab depressurisation systems design, Build. Environ. 42 (2007) 1994–2003, https://doi.org/10.1016/j.buildenv.2006.04.002.
[57] I. López Coto, J.L. Mas, J.P. Bolivar, R. García-Tenorio, A short-time method to measure the radon potential of porous materials, Appl. Radiat. 67 (2009) 133–138, https://doi.org/10.1016/j.apradiso.2008.07.015.
[58] I. Gutiérrez-Álvarez, J.E. Martín, J.A. Adame, C. Grossi, A. Vargas, J.P. Bolívar, Applicability of the closed-circuit accumulation chamber technique to measure radon surface exhalation rate under laboratory conditions, Radiat. Meas. 133 (2020) 106284, https://doi.org/10.1016/j.radmeas.2020.106284.
[59] D.V. Hutton, Fundamentals of Finite Element Analysis, 2004, Hutton, 2004.
[60] R.L. Taylor, The Finite Element Method Fifth Edition Volume 1: The Basis, 2000.
[61] K. Debertin, R.G. Helmer, Gamma and X ray Spectrometry with Semiconductor Detector, 1988.
[62] Murray R. Spiegel, Estadistica-Schaum, 1970.
[63] R.P. Chauhan, A. Kumar, A comparative study of indoor radon contributed by diffusive and advective transport through intact concrete, Phys. Procedia (2015) 109–112, https://doi.org/10.1016/j.phpro.2015.11.066.
[64] R.P. Chauhan, A. Kumar, Study of radon transport through concrete modified with silica fume, Radiat. Meas. 59 (2013) 59–65, https://doi.org/10.1016/j.radmeas.2013.10.009.
[65] R.P. Chauhan, A. Kumar, Radon resistant potential of concrete manufactured using Ordinary Portland Cement blended with rice husk ash, Atmos. Environ. 81 (2013) 413–420, https://doi.org/10.1016/j.atmosenv.2013.09.024.
[66] A. Kumar, R.P. Chauhan, Active and passive measurements of radon diffusion coefficient from building construction materials, Environ. Earth Sci. 72 (2014) 251–257, https://doi.org/10.1007/s12665-013-2951-5.
[67] G. Keller, B. Hoffmann, T. Feigenspan, Radon permeability and radon exhalation of building materials, Sci. Total Environ. 272 (2001) 8589, https://doi.org/10.1016/s0048-9697(01)00669-6.